Chapter 3
Carbon Dioxide Separation, Capture, and Storage in Porous Materials

Anita Das, Deanna M. D'Alessandro and Vanessa K. Peterson

Abstract Solid porous materials represent one of the most promising technologies for separating and storing gases of importance in the generation and use of energy. Understanding the fundamental interaction of guest molecules such as carbon dioxide in porous hosts is crucial for progressing materials towards industrial use in post and pre combustion carbon-capture processes, as well as in natural-gas sweetening. Neutron scattering has played a significant role already in providing an understanding of the working mechanisms of these materials, which are still in their infancy for such applications. This chapter gives examples of insights into the working mechanisms of porous solid adsorbents gained by neutron scattering, such as the nature of the interaction of carbon dioxide and other guest molecules with the host as well as the host response. The synthesis of many of these porous hosts affords significant molecular-level engineering of solid architectures and chemical functionalities that in turn control gas selectivity. When directed by the insights gained through neutron-scattering measurements, these materials are leading toward ideal gas separation and storage properties.

3.1 The Importance of Carbon Dioxide Capture

As the prime mover of carbon through the atmosphere, carbon dioxide (CO_2), plays a vital role in enabling the cycle of carbon from the Earth's crust (where it is found in elemental graphite and diamond, carbonates, and fossil fuels) to our oceans

A. Das · D.M. D'Alessandro (✉)
School of Chemistry, The University of Sydney, Sydney, NSW, Australia
e-mail: deanna.dalessandro@sydney.edu.au

A. Das
e-mail: anita.das@sydney.edu.au

V.K. Peterson (✉)
Australian Nuclear Science and Technology Organisation, Lucas Heights, NSW, Australia
e-mail: vanessa.peterson@ansto.gov.au

G.J. Kearley and V.K. Peterson (eds.), *Neutron Applications in Materials for Energy*, Neutron Scattering Applications and Techniques,
DOI 10.1007/978-3-319-06656-1_3

(where it occurs in carbonate minerals formed by the action of coral-reef organisms and aqueous CO_2). For hundreds of millions of years, the carbon cycle has maintained a relatively constant amount of CO_2 in the Earth's atmosphere (approximately 400 ppm by volume). While the contribution from human industry is relatively small, its recent growth has shifted this natural balance. Since the start of the Industrial Revolution around 1760, the concentration of CO_2 in the atmosphere has risen dramatically from 280 to 385 ppm today [1, 2]. This significant rise has been attributed to an increasing dependence on the combustion of fossil fuels (coal, petroleum, and natural gas), which account for 86 % of man-made greenhouse-gas emissions, the remainder arising from land use change (primarily deforestation) and chemical processing.

The development of more efficient processes for CO_2 capture from major point sources such as power plants and natural-gas wells is considered a key to the reduction of greenhouse-gas emissions implicated in global warming. Numerous national and international governments and industries have established collaborative initiatives such as the Intergovernmental Panel on Climate Change [3] (IPCC), the United Nations Framework Convention on Climate Change [4], and the Global Climate Change Initiative [5] to achieve this goal. The capture and sequestration of CO_2, the predominant greenhouse gas, is a central strategy in these programmes as it offers the opportunity to meet increasing demands for fossil-fuel energy in the short to medium term, whilst reducing the associated greenhouse-gas emissions in line with global targets. Carbon capture and storage (CCS) will complement other strategies such as improving energy efficiency, switching to less carbon-intensive fuels, and the phasing in of renewable-energy technologies.

Three major technologies are predicted to have the greatest likelihood of reducing man-made emissions to the atmosphere that are implicated in global warming. These processes include postcombustion and precombustion capture from power plants involving $CO_2/N_2/H_2O$ and CO_2/H_2 separations, respectively, and natural-gas sweetening ($CO_2/CH_4/N_2$ separation). The separation processes required for each of these capture applications differs with regard to the nature of the gas mixture and the temperatures and pressures involved, imposing constraints on the materials and processes employed [6, 7].

Conventional CO_2 capture processes employed in power plants world-wide are typically postcombustion 'wet scrubbing' methods, involving the absorption of CO_2 by amine-containing solvents such as methanolamines [8]. Power plant flue-gas streams consist primarily of N_2, H_2O, and CO_2 in a 13:2:2 ratio by weight [9]. Prior to the compression and liquefication of the captured CO_2 for transportation to storage sites, CCS requires the separation of CO_2 from all other flue-gas components. CO_2 is strongly absorbed by the amine to form a carbamate species [10], however, the high heat of formation associated with the creation of the carbamate leads to a considerable energy penalty for regeneration of the solvent. Since the flue streams from coal-fired power plants contain dilute concentrations of CO_2 (typically 10–15 %) at relatively low pressures and temperatures (1 atm., 40 °C), it is estimated that CO_2 capture and compression will increase the energy requirements of a plant by 25–40 %. Analysis has shown that the thermodynamic minimum energy-penalty

for capturing 90 % of the CO_2 from the flue gas of a typical coal-fired power plant is approximately 3.5 % (assuming a flue gas containing 12–15 % CO_2 at 40 °C) [11]. The transportation and storage of CO_2 will necessitate further investment and capital costs. These economic and energy comparisons underscore the immense opportunities and incentives that exist for improved CO_2 capture processes and materials. Despite improvements in conventional postcombustion chemical-absorption methods, wet-scrubbing methods suffer a number of drawbacks and are therefore not cost-effective for large-scale carbon emissions reduction.

While the retrofitting of existing power plants using postcombustion capture methods presents the closest marketable technology, two major alternatives to postcombustion CO_2 capture processes have been proposed, and are currently in the test stages of development [12]. Precombustion processes involve a preliminary fuel-conversion step using a gasification process and subsequent shift-reaction to form a mixture of CO_2 and H_2 prior to combustion. The high pressure of the product gas-stream facilitates the removal of CO_2 from the CO_2/H_2 mixture at pressures of 30–50 bar and temperatures of 50–75 °C [13]. The significant advantage of precombustion capture is that the higher component concentrations and elevated pressures reduce the energy capture penalty of the process to 10–16 %, roughly half that for postcombustion CO_2 capture. A further advantage is that precombustion technology generates an H_2-rich fuel, which can be used as a chemical feedstock in a fuel cell for power generation or in the development of an H_2 economy. In oxyfuel (or denitrogenation) processes, fuel is combusted in O_2 instead of air by the exclusion of N_2, thereby producing a concentrated stream of CO_2 without the need for separation (in high, sequestration-ready concentrations of 80–98 %). Since the separation of interest in this case is air separation (O_2 from mainly N_2 at a pressure of around 100 bar and temperature of 50 °C), reducing the cost of O_2 generation is key to industrial viability. While the emerging technologies associated with precombustion and oxyfuel processes cannot be readily incorporated (via retrofitting) into existing power plants as can postcombustion CO_2 capture processes, the projections from the IPCC indicate that the required extensive capital investments will be compensated by the relatively higher efficiency of the CO_2 separation and capture process [3].

Another important application for CO_2 capture technologies is the ‘sweetening’ of sour natural-gas wells, where the sweetening refers to the separation of CO_2 from CH_4. Natural gas reserves (mainly CH_4) are typically contaminated with over 40 % CO_2 and N_2 and the use of such fields is only acceptable if the additional CO_2 is separated and sequestered at the source of production. The capture of CO_2 from ambient air has also been suggested, however, the low concentration of CO_2 in air (0.04 %) presents a significantly higher barrier to capture compared with postcombustion methods, and the expense of moving large volumes of air through an absorbing material presents a further challenge in its implementation [6].

The key factor that underscores significant advancements in CCS is materials to perform the capture process [6, 7]. The challenge for gas-separation materials is that the differences in properties between the gases that have to be separated are relatively small. However, differences do exist in the electronic properties of the gases:

CO_2 has a large quadrupole moment (13.4×10^{-40} cm^2 vs. 4.7×10^{-40} cm^2 for N_2 and CH_4 is non-polar) and CH_4 adsorbs preferentially over N_2 due to its higher polarizability (17.6×10^{-25} cm^3 for N_2 and 26.0×10^{-25} cm^3 for CH_4).

A diverse range of promising methods and materials for CO_2 capture applications that could be employed in any one of the abovementioned postcombustion, precombustion, or oxyfuel processes have been proposed as alternatives to conventional chemical absorption. These include the use of physical absorbents, membranes, cryogenic distillation, hydrate formation, chemical-looping combustion using metal oxides, and adsorption on solids using pressure and/or temperature swing adsorption, where the adsorption and desorption temperature/pressures are different and a "swing" is made between them [14]. The key requirements for these new materials are that they exhibit air and water stability, corrosion resistance, high thermal-stability, high selectivity and adsorption capacity for CO_2, as well as adequate robustness and mechanical strength to withstand repeated exposure to high-pressure gas streams. A number of review articles have elaborated the status of a new classes of materials for CO_2 capture [6, 7]. In particular, metal-organic framework (MOF) materials are progressing at a rapid pace.

With respect to new materials, the key scientific challenges are the development of a level of molecular control and modern experimental and computational methods. For crystalline materials, adsorption isotherms and breakthrough–curve measurements under conditions that closely resemble working-condition gas mixtures are essential. In reality, pure gas-adsorption isotherms are often measured, with ideal adsorbed solution theory (IAST) applied in some cases to predict multicomponent adsorption behaviour [15]. A parameter that must be assessed in all cases is the enthalpy of adsorption, since the cost for the regeneration of a capture material is clearly dependent on the energy required to remove the captured CO_2.

Characterization of the molecular transport properties of materials is essential to obtain an understanding of transport processes. Important molecular-level information required includes: how the material structure changes with loading, how adsorbates bind to the material, and how different permeates influence each other's solubility. In situ techniques are particularly powerful as they allow the interactions between gas molecules and the matrix to be probed and determine the material structure under different loading conditions. The most significant information from such measurements is gained from the ability to correlate absorbate uptake with the absorbent structure and the molecular-level absorbate mobility. A comparison between the molecular-level absorbate mobility and its macroscopic diffusion should provide insights into the mechanism of selective transport through these materials.

In parallel with experimental studies, computational modelling methods are being developed, both as a tool to understand further details of the adorbate-absorbent interaction, and as a tool to predict the performance of materials proposed for a given separation process, with the latter enabling large-scale screening of new materials. Ultimately, a clear understanding of the structure- and dynamics-function relations will direct experimental efforts towards a new generation of materials with

improved CO_2 capture abilities. Developing force fields for computational work using detailed structures is important for the successful prediction of thermodynamic and transport properties of new materials.

3.1.1 Porous Materials for CO_2 Separation and Storage

Microporous and mesoporous solid-state materials such as activated carbon, carbon-based molecular sieves, mesoporous silicas, and zeolites have been demonstrated to have a significant, and in some cases selective, CO_2 adsorption capacity. Such materials have advantages for CO_2 capture over the amine solvents currently employed in industry as they are endowed with better stabilities and lower energies of regeneration. Zeolites in particular have been widely studied for the purpose of CO_2 capture due to their defined and controllable pore size, insensitivity to moisture, and high uptake at non-extreme conditions (for example, zeolite 13X has a CO_2 uptake of 3.6 mmol.g^{-1} at 25 °C) [16]. At higher, more industrially-relevant temperatures, these zeolites tend to lose adsorption capacity and also suffer low selectivity for CO_2 over other gases (e.g. N_2 and H_2) as a result of the physisorptive nature of the CO_2-adsorbate interaction. To enhance selectivity for CO_2, amine-impregnated or amine-modified materials have been explored, which couple the chemisorption approach used in conventional liquid-amine capture with the physisorption approach traditionally seen in porous solid materials. This technique has also been employed using a number of porous silicas, such as MCM-41 mesoporous molecular sieves impregnated with polyethylenimine [17] and SBA-15 mesoporous silicas covalently tethered with hyperbranched amines [18]. Despite the increase in CO_2 selectivity of such materials achieved using this approach, they often suffer low stabilities over repeated cycles.

For industrial purposes, solid materials with high selectivity and capacity for CO_2 uptake, as well as stability to extreme industrial conditions and a low energy for regeneration, are desired. Metal-organic frameworks (MOFs) are a highly promising class of material for this application due to their structural and chemical versatility, arising from different combinations of metal coordination-spheres as well as multidentate bridging ligands with different lengths, shapes, and directionalities of the coordinating groups. While this versatility sometimes comes at the expense of being able to predict structure accurately, the MOF scaffold provides a unique platform upon which to systematically tune the functionalities of known structures to obtain a desirable property [19]. They may be rationally engineered to have a high surface area and porosity, can be post-synthetically modified to allow for increased selectivity for CO_2, and can possess excellent stability under industrially-relevant conditions [20]. High surface areas and the possibility to possess coordinatively-unsaturated metal sites make MOFs particularly attractive as gas-selective adsorbents. Coordinatively-unsaturated metal centres have been generated in such materials via chelation by post-synthetically modifying bridging ligands or via insertion into open-ligand sites [9]. However, they are most often created

through the evacuation of MOFs that have metal-bound solvent molecules. An effective strategy in tuning the selectivity of MOFs for CO_2 is the introduction of functional groups into the pores such as amine [21, 22] and sulfone groups (a SO_2 group attached to two C atoms) [23], known to specifically interact with CO_2 preferentially over other gases of industrial interest.

Topological control is another strategy employed in the design of MOFs for gas separation, however, this approach is frequently serendipitous due to unknown mechanisms of formation of these materials. Despite this, it has been shown that pore size and shape modulation can determine the diffusion dynamics of the molecules to be separated (e.g. metal formates, $M(HCO_2)_2$ (M = Mg, Mn, Co, or Ni), have been shown to selectively adsorb CO_2 over CH_4, suggesting a size-exclusion effect by the small pores) [24]. Generally, attempts to increase pore size through the incorporation of longer ligands results in framework interpenetration. While this is disadvantageous from a gas-storage standpoint, it may be favourable for some guest separations by their kinetic-diameter differences (e.g. CO_2 over CH_4) [25, 26]. This type of "molecular sieving" approach may also be achieved by taking advantage of the structural flexibility in MOFs. For example, the material Cr(OH)(bdc), where bdc = 1, 4-benzenedicarboxylate and also known as MIL-53(Cr), exhibits a two-step CO_2 uptake isotherm compared to a single-step CH_4 uptake isotherm, indicative of a specific "gating" effect [27].

3.2 Neutron Scattering in Studying Porous Materials for CO_2 Separation and Storage

Neutron scattering holds many opportunities for obtaining unique information concerning the porous-solid adsorbent (host) as well as host-adsorbate (host-guest) system. Measurement of structure and dynamics using neutron scattering, across length and time scales pertinent to these systems (also possible at the same time), has been exploited for the better understanding of guest binding in the host and separation mechanisms, as well as the host's response to adsorption, all of which are key to progressing the application of such systems in CCS.

Information about both host and host-guest structure, which yields details of the structural response of the host to adsorption, the location of the guest in the host, and guest-host interaction, are important to determining structure-property relations. As neutron diffraction intensity does not reduce with scattering angle, relatively more fine structural detail is gained than using X-ray diffraction, providing important detail concerning the guest–host and guest–guest interactions. The isotopically-dependent structural information afforded by neutrons allows different contrast between parts of the host framework and/or guest to be gained, providing many advantages for such structural investigations. Examples include distinguishing between guests such as N_2, O_2, and CO_2, and obtaining details of both the host's ligands and metal centres, as well as guests, even within a MOF containing heavy-metal atoms and guests containing light atoms. Additionally, the information

obtained can be tuned through isotopic substitution, such as in determining the molecular orientations of CH_4 within a host using the isotopically-substituted CD_4, where D is deuterium (^2H),

The dynamic information obtained through neutron scattering is also isotopically dependent, and spectroscopic neutron techniques allow direct measurement of the local environment and the diffusional transport of the guest within the host. Both structure and dynamics can be measured at the same time, enabling insights into the geometry of the guest motion, in turn allowing the details of the mechanism of diffusion of the guest within the host to be gained.

In situ methods are central in the analysis of MOFs for guest separation and storage applications. Although in situ X-ray single crystal and powder diffraction studies of CO_2 in MOFs facilitate the understanding of the functional mechanism of MOFs for CCS applications [28–30], in situ neutron-scattering methods have significant advantages over X-ray studies of MOF-guest systems, with the penetrating power of neutrons being central to this. Neutrons easily penetrate the often-complex sample environments required for control over temperature of the host at the same time as gas delivery, covering easily the range of temperatures from the relatively cold (about −263 °C) conditions required to "lock in" guests and determine accurate structural details, to the more moderate temperatures required to replicate working post-, pre-, and oxyfuel combustion, as well as natural gas-sweetening conditions (40–75 °C). The relatively high penetrating power of neutrons also allows for the analysis of bulk samples, mg—gram quantities, providing information about the more industrially-relevant "bulk" properties of the material. The bulk-scale analysis also aids in accurately dosing the sample with a known number of guest molecules to determine in detail the nature of their interaction with the host.

3.2.1 Location of CO_2

Neutron powder diffraction (NPD) has been used extensively to determine the location of guest molecules in porous framework materials, and this work extends to CO_2 [31–36]. Two MOFs that have been explored intensively for their selective sorption properties are M_2(dobdc) (M = Mg, Mn, Co, Ni, Zn; dobdc = 2, 5-dioxido-1, 4-benzenedicarboxylate), also known as MOF-74 or CPO-27, and $M_3(btc)_2$ (M = Cu, Cr, Mo; btc = 1, 3, 5-benzenetricarboxylate) with $Cu_3(btc)_2$ also known as HKUST-1. Both materials contain exposed M^{2+} sites, with the M_2(dobdc) material possessing exceptionally large densities of such sites. The location of CO_2 in the two MOF materials Mg_2(dobdc) and $Cu_3(btc)_2$, along with the host–CO_2 structure, was determined using NPD. The nature of the host–CO_2 interaction in both materials was identified to be binding at metal sites via an oxygen with the remainder of the molecule remaining relatively free (see Fig. 3.1), where the adsorbed CO_2 is clearly located above the open Mg ions in Mg_2(dobdc) [32]. Importantly, the presence of coordinatively-unsaturated metal sites in MOFs such as M_2(dobdc) and $Cu_3(btc)_2$ leads to enhanced interactions between adsorbates such

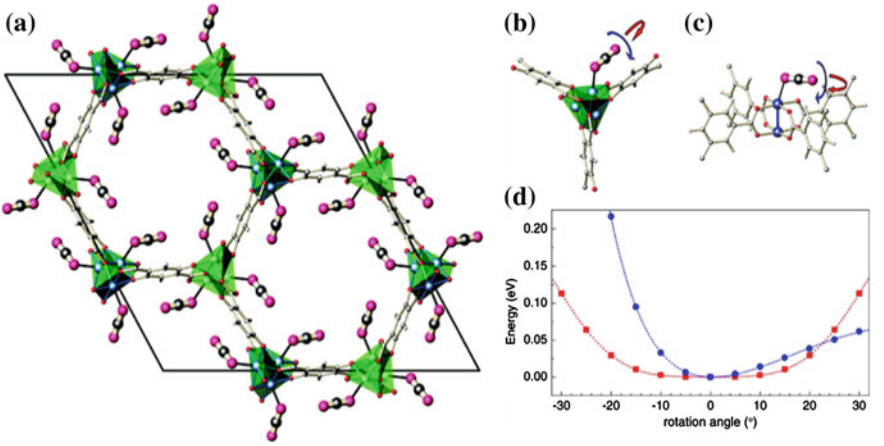

Fig. 3.1 **a** $Mg_2(dobdc)$-CO_2 structure determined from NPD showing the strongest CO_2 binding-site. (**b–c**) Schematic showing the dominant two motions of the CO_2 at the open metal, determined from computational calculations using the NPD-derived structures for $Mg_2(dobdc)$ (**b**) and $Cu_3(btc)_2$ (**c**). Arrows in (**b–c**) represent CO_2 motions occurring about the surface normal largely parallel to the metal—O plane (*red*) and away from this surface normal (*blue*). The potential energy for these two modes occurring in $Cu_3(btc)_2$ is shown (**d**) as a function of CO_2 rotation angle. Atomic structure is represented with Mg and O forming the central polyhedra (**a**) in $Mg_2(dobdc)$ and (axial pair) in $Cu_3(btc)_2$ (**c**), with C and H forming the linker, and the pendant CO_2 (**a**). Reprinted with permission from (H. Wu, J.M. Simmons, G. Srinivas, W. Zhou, T. Yildirim, J. Phys. Chem. Lett. **1**, 1946 (2010)) [37]. Copyright (2010) American Chemical Society

as CO_2 and the host framework, but also guest molecules such as CH_4 and H_2. Indeed, we will show that the application of NPD to examine competitive binding between CO_2 and these other gases represents an area of significant current interest.

Density-functional theory (DFT) calculations performed using the NPD-determined structures allowed evaluation of the representative CO_2 motions in $Mg_2(dobdc)$ and $Cu_3(btc)_2$. These calculations show that the O bound to the open metal can be approximated as the rotational centre. In both materials the open metal and the associated carboxyls from the ligands form a nearly square-planar surface at the CO_2 binding-site, such that the metal–CO_2 interaction closely represents a surface normal. The CO_2 rotations are shown by arrows in Fig. 3.1(b–c), occurring about the surface normal (red arrows) and away from the surface-normal (blue arrows). The mode energies for the motions denoted by the red and blue arrows are 4.3 and 8.5 meV for $Mg_2(dobdc)$, respectively, and 0.2 and 3.4 meV for $Cu_3(btc)_2$, respectively. To gain more direct information about the CO_2-host interaction in $Cu_3(btc)_2$ the energy at the open-metal sites (assuming a rigid host framework) was calculated for these two CO_2 motions as a function of CO_2 rotational angle, and is shown in Fig. 3.1d. As expected, the energy curves are shallow, particularly in the ±10° region, allowing for significant CO_2 orientational disorder in the MOF at this site with little effect on the total energy of the MOF–CO_2 system. These findings are in excellent agreement with the relatively-large atomic displacement

parameters of CO_2 adsorbed at open metal sites obtained from the NPD measurements, in particular for $Cu_3(btc)_2$. These results also point to the presence of disorder (either static or dynamic) in the orientation of the CO_2 molecule, resulting in a relatively large apparent O–C–O bond bend obtained from the NPD data, which is a structural average and strongly biased by the relatively large disorder of the adsorbed CO_2. Since CO_2 is reversibly physisorbed on these open metal sites, a large degree of CO_2 bond activation and bending is unlikely.

Vacancy-containing Prussian blue analogues of the formula $M(1)^{II}{}_3[M(2)^{III}(CN)_6]^2$ (where M(1) and M(2) are transition metals) are excellent candidate gas adsorbents as 1/3 of their octahedral $M^{III}(CN)_6^{3-}$ units are vacant for charge neutrality, generating both non-vacancy and vacancy pores. Each vacancy pore will possess some of the six bare-metal sites per formula unit (eight per unit cell). The $M(1)_3[Co(CN)_6]_2$ system (M(1) = Mn, Co, Ni, Cu, Zn, Fig. 3.2) displays good selectivity for CO_2 over CH_4 and N_2 [38], with a NPD study revealing two sites for CO_2 binding in the $Fe_3[Co(CN)_6]_2$ material, which has a CO_2 uptake of

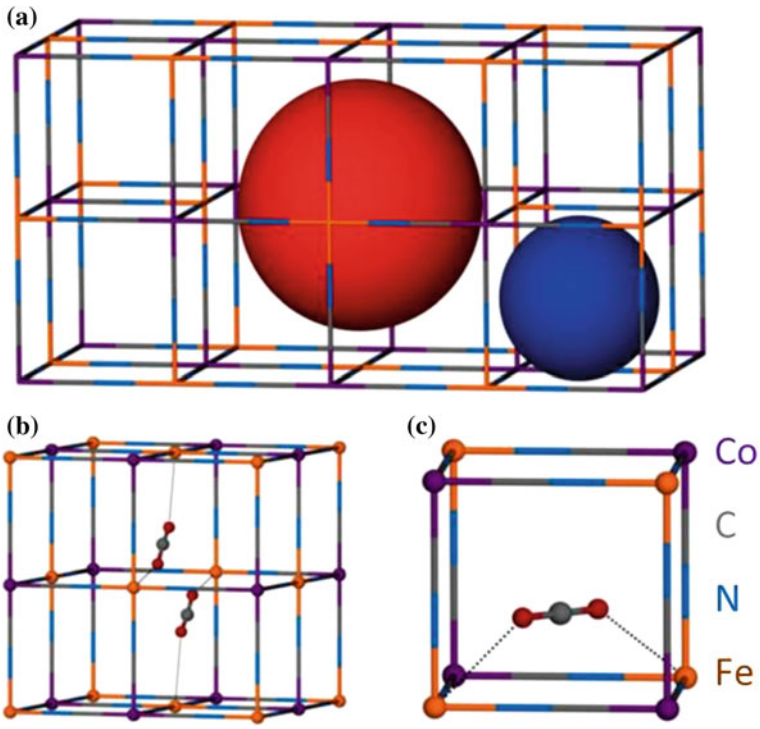

Fig. 3.2 **a** $Fe_3[Co(CN)_6]_2$ structure showing non-vacancy (*right sphere*) and vacancy (*left sphere*) pores. **b** Bridging open-metal CO_2 adsorption site located in a vacancy-type pore. **c** Non open-metal interacting CO_2 adsorption site located above non-vacancy square faces of the framework. Reproduced from (S.H. Ogilvie, S.G. Duyker, P.D. Southon, V.K. Peterson, C.J. Kepert, Chem. Commun. **49**, 9404 (2013)) [39]

2.20 mmol g^{-1} at 35 °C and 1 bar [39]. At one of these sites CO_2 was found to bridge between two open-metal sites, with the quadrupolar CO_2 molecule interacting strongly with the positively-charged Fe sites. The saturation of this site by CO_2 at relatively-low CO_2 concentrations indicated the favourable nature of the interaction, explaining the selectivity of the material.

CO_2 hydrates, consisting of an H_2O-cage encapsulating a CO_2, are another porous material that have great potential for application as CO_2 adsorbents, and these too have been studied using NPD to determine the locations of CO_2 within the cage [40]. This study used a cage in which D was substituted for H, allowing structural details of the cage atoms and their interaction with the CO_2 to be determined. The study also included the temperature-dependence of this CO_2-cage interaction. Data indicate that the CO_2 molecule in the tetrakaidecahedral cage rotates rapidly even at low temperatures and that the interaction between the CO_2 molecule and the D atoms of the cage is strong enough to provide the site dependence of the atomic displacement parameters of the D atoms. Further work on CO_2 hydrates [41] using NPD found CO_2 to have different motions in the small and large cages of this system. In both cages the CO_2 resides at the cage centre, however, in the small cage the O atoms revolved freely around the C atom, in contrast to the large cage where the O atoms revolved around the C atom along the plane parallel to the hexagonal facets of the cage. The analysis of CO_2 hydrates using NPD has also been extended to studies of their formation, including kinetics, using in situ NPD [42]. This work also derived the occupancy of CO_2 in the small and large cage during the formation of the hydrate.

3.2.2 Dynamics of the CO_2-Host System

Crystallographic studies provide the time-averaged position of atoms, and whilst some insight into atom dynamics can be gained through analysis of the average structure and atomic displacement parameters, detailed information regarding the dynamics of the guest and host-guest system are better gained through other neutron-scattering methods. Inelastic neutron scattering (INS) combined with computational calculations permit visualization of the atom dynamics and allow elucidation of the interaction between adsorbed guest molecules and the host.

Measurement of the interaction between CO_2 molecules and the porous host is crucial to understanding the detailed binding mechanism and therefore the observed selectivity and guest-uptake properties of porous hosts. INS cannot directly detect the CO_2 binding interaction within an adsorbent because the incoherent neutron-scattering cross section for these elements (for their naturally-abundant isotopes) is effectively zero, being 0.001 barns each. One approach to overcome this problem is to combine INS and DFT to visualize captured CO_2 molecules within a porous host by investigating the change in the dynamics of the other atoms of the adsorbent structure. INS spectra can be calculated directly using DFT-based computations to obtain the force constants, and then making the harmonic approximation to obtain

the eigenvectors and eigenvalues to determine the spectral intensities and frequencies, respectively [43]. INS and DFT-based calculations are a powerful combination in understanding the working mechanism of functionalized materials containing specific gas molecule binding-sites, probing directly the impact of functional groups, and other host features such as topology and pore shape and size on the orientation and type of binding of CO_2 in the host.

An example of this is the application of INS and DFT to study CO_2 in the material $Al_2(OH)_2$(bptc), where bptc = biphenyl-3, 3′,5, 5′-tetracarboxylate and also known as NOTT-300, where the neutron-scattering signal comes primarily from the H atoms in the $Al_2(OH)_2$(bptc) hydroxyl groups and benzene rings of the ligand, and the INS signal is perturbed by the binding of CO_2 (Fig. 3.3) [44]. $Al_2(OH)_2$(bptc) is an Al-hydroxyl functionalized porous-solid exhibiting high chemical and thermal stability as well as high selectivity and uptake capacity for CO_2 and SO_2. The

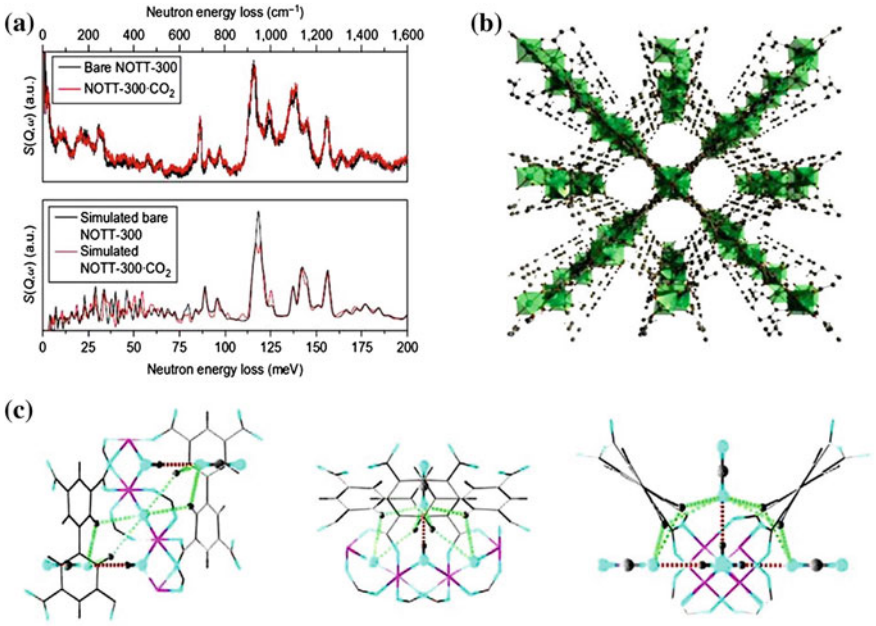

Fig. 3.3 **a** Experimental (*top*) and DFT-simulated (*bottom*) INS spectra for bare and CO_2-loaded $Al_2(OH)_2$(bptc), also known as NOTT-300. **b** View of the three-dimensional framework structure showing channels along the *c*-axis (into the page). Water molecules in the channel are omitted for clarity. **c** Detailed views of –OH and –CH groups binding CO_2 in the "pocket" cavity of CO_2-loaded $Al_2(OH)_2$(bptc). Views along the *a*-axis (left), the *b*-axis (*centre*), and the *c*-axis (*right*). The moderate hydrogen bond between O(δ-) of CO_2 and H(δ^+) of –OH is dotted *red* (O–H = 2.335 Å). The weak cooperative H bond between the O(δ^-) of CO_2 and the H(δ^+) from the –CH is dotted green (O—H = 3.029, 3.190 Å with each occurring twice), indicating that each O(δ^-) centre interacts with five different H(δ^+) centres. Reprinted with permission from (S. Yang, J. Sun, A.J. Ramirez-Cuesta, S.K. Callear, W.I.F. David, D.P. Anderson, R. Newby, A.J. Blake, J.E. Parker, C.C. Tang, M. Schröder, Nat. Chem. **4**, 887 (2012)) [44]. Nature Publishing Group

material exhibits no apparent adsorption of H_2 and N_2, which is attributed to the slow diffusion of these gases through the narrow pore channels. In contrast, unusually high and selective CO_2 and SO_2 uptakes were observed, including at low-pressure. The INS spectra revealed two major increases in peak intensity upon adsorption of 1.0 CO_2 into the formula unit: peak I at lower energy transfers (30 meV) and peak II at higher energy transfer (125 meV). Peaks in the range 100–160 meV were slightly shifted to higher energies in the CO_2-adsorbed material, indicating a hardening of the motion of the $Al_2(OH)_2$(bptc) host upon CO_2 adsorption.

The INS spectrum derived from DFT calculations show good agreement with the experimental spectrum and confirm that the adsorbed CO_2 molecules are located end-on to the hydroxyl groups. The O–H distance between the CO_2 molecule and the hydroxyl group is 2.335 Å, indicating a moderate to weak hydrogen bond, with the optimized C–O bond distances in CO_2 being 1.183 Å at the hydrogen-bonded end and 1.178 Å at the free end. The CO_2 is linear with a O–C–O bond angle of 180°. Each adsorbed CO_2 molecule is found to be surrounded by four aromatic C–H groups, forming weak cooperative supramolecular interactions between the O(δ^-) of the CO_2 and the H(δ^+) of the –CH (where O–H = 3.029 and 3.190 Å and each occurs twice). Peak I in the INS spectrum was assigned to the O–H group wag, occurring perpendicular to the Al–O–Al direction and attributed to the presence of the CO_2. Peak II in the spectrum was assigned to the wag of the four aromatic C–H groups on four benzene rings adjacent to each CO_2, in conjunction with the OH group wag. Hence, in this work the direct visualization of host–guest interactions through INS and DFT calculations was crucial in rationalizing the material's high selectivity for CO_2 and in understanding the detailed binding mechanism of CO_2 in the material. The low H_2 uptake of the material was rationalised in a similar manner, with the contribution from H_2 in the material to the INS data, consistent with that expected for liquid H_2, indicating a weak interaction with the material.

3.2.3 Diffusion and Transport of CO_2

Application of quasielastic neutron scattering (QENS) in tandem with molecular dynamics (MD) simulations brings insights into the dynamics and transport of CO_2 in porous media [45]. Whilst the self-diffusion of molecules containing atoms that have appreciable incoherent neutron-scattering cross sections can be measured directly using QENS, the neutron-scattering cross section of CO_2 is coherent and so the coherent QENS approach must be used to monitor the CO_2 and the transport diffusivity extracted from this. Comparisons between MD simulation and QENS experiments involve the diffusing molecule's self-diffusivity, however, in practical separations and catalytic applications, it is the transport diffusivity that is of greater importance. The transport diffusivity involves the response to a chemical potential gradient and its direct determination calls for non-equilibrium experiments. At the molecular level the dependence of the transport diffusivity and the so-called corrected diffusivity needs to be resolved. Linear response theory allows the transport

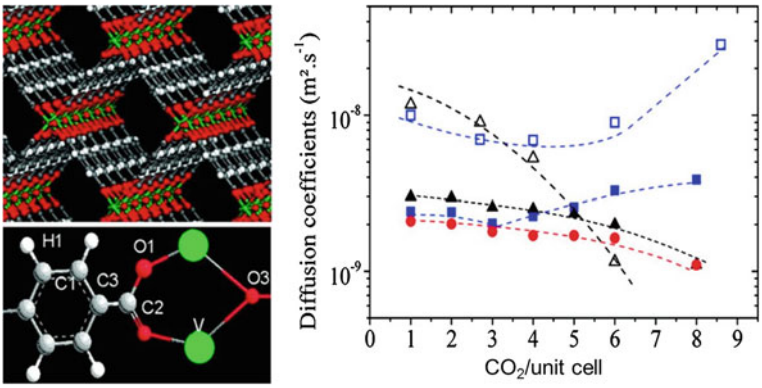

Fig. 3.4 *Left* The orthorhombic (*Pnma*) V(O)(bdc) structure displayed along the z axis, highlighting the one-dimensional pore system (*top*). Labels of the different atoms of the V(O)(bdc) structure (*bottom*). *Right* Evolution of the experimental diffusion coefficients (corrected = △ and transport = □) and simulated diffusion coefficients (self = ●, corrected = ▲, and transport = △) as a function of the CO_2 concentration in V(O)(bdc). The error bars for the simulations are 16, 7, and 12 % for low, intermediate, and high loading, respectively, while the experimental data are defined within an average error bar of 20 %. Reprinted with permission from (F. Salles, H. Jobic, T. Devic, P.L. Llewellyn, C. Serre, G. Ferey, G. Maurin, ACS Nano **4**, 143 (2010)) [48]. Copyright (2010) American Chemical Society

and corrected diffusivity to be determined directly under equilibrium conditions, where chemical potential gradients are absent. Chapter 2 contains details of the relationship between the self-diffusivity, as measured using incoherent QENS, and the transport diffusivity, D_t, as derived from coherent neutron-scattering. Experimentally, this objective can be accomplished by using coherent QENS, which probes the collective motion of guest molecules at equilibrium [46]. The same objective can be accomplished using equilibrium MD simulations.

The joint MD-experimental QENS approach in which simulated CO_2 dynamic properties are validated allows further details of the CO_2 dynamics and transport in the host to be obtained, such as first demonstrated for CO_2 in the NaX and NaY faujasite zeolites [47]. The joint coherent QENS-MD approach was first applied to MOFs in the study of the isostructural Cr(OH)(bdc) and V(O)(bdc) materials and also known as MIL-53(Cr) and MIL-47(V), respectively [48, 49]. This work built on the study of H_2 self-diffusion in these materials as detailed in Chap. 2. V(O)(bdc) contains corner-sharing $V^{4+}O_4O_2$ octahedra connected by bdc linker groups yielding one-dimensional channels (Fig. 3.4). Consequently, V(O)(bdc) has a relatively-high working capacity for CO_2 uptake with moderate selectivity for CO_2 in the absence of functional groups within the channel wall. The concentration-dependent self corrected (calculated from MD) and transport diffusivities (measured using QENS) of CO_2 in the rigid V(O)(bdc) material were determined [48], revealing the three-dimensional diffusion of CO_2 through the channels.

Cr(OH)(bdc) differs from V(O)(bdc) by the substitution of μ_2–O groups located at the M–O–M links in V(O)(bdc) by μ_2–OH groups in Cr(OH)(bdc). This

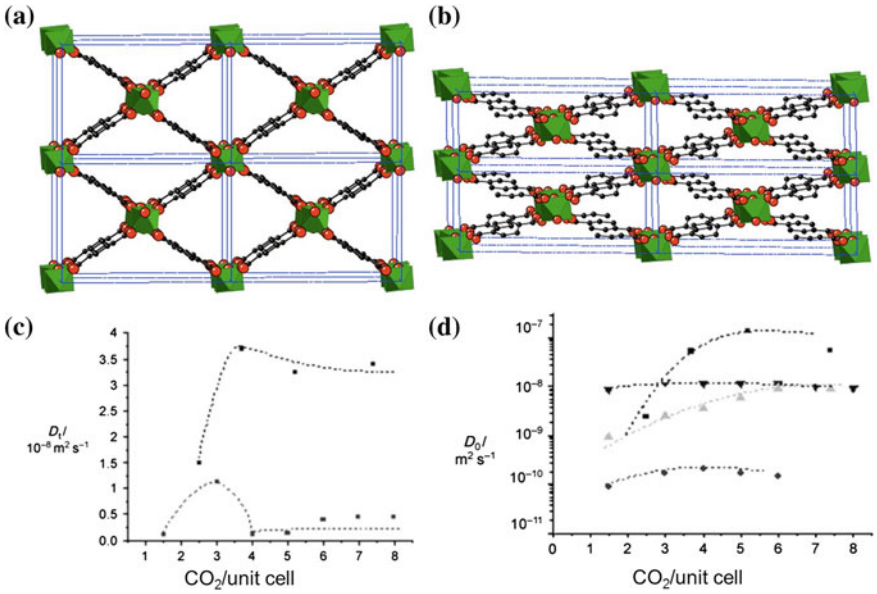

Fig. 3.5 Structural switching of the Cr(OH)(bdc) system induced by CO_2 adsorption between large-pore (*Imcm*) (**a**) and narrow-pore (*C*2/*c*) (**b**) forms. Experimental (**c**) and simulated (**d**) transport diffusivity (D_t) as a function of CO_2 concentration. Corrected diffusivities (D_0) simulated for the rigid narrow (•) and large pore (▼) forms, along with D_0 simulated using a composite approach (▲) and experimentally determined (■). Top: Reprinted with permission from (A.V. Neimark, F.-X.Coudert, C. Triguero, A. Boutin, A.H. Fuchs, I. Beurroies, R. Denoyel, Langmuir **27**, 4734 (2011)) [50]. Copyright (2011) American Chemical Society. Bottom: Reprinted from (F. Salles, H. Jobic, A. Ghoufi, P.L. Llewellyn, C. Serre, S. Bourrelly, G. Ferey, G. Maurin. Angew. Chem. Int. Edition **48**, 8335 (2009)) [49]

difference makes Cr(OH)(bdc) highly selective for CO_2, in a specific pressure range, which is a consequence of the large-scale breathing modes exhibited by the material. This allows it to switch from a large pore (LP) form to a narrow pore (NP) structure upon CO_2/CH_4 adsorption, with the NP structure able to trap CO_2 and not CH_4. As with the V(O)(bdc) study, the combined coherent QENS-MD approach was used to study the concentration-dependent self- and transport diffusion of CO_2 in Cr(OH)(bdc). This work found a single-file diffusion regime in the material at high CO_2 loading, a phenomenon not previously shown for any MOF (Fig. 3.5).

3.2.4 Evolution of Microstructure of the Host and Adsorption Capacity

Large-scale structure analysis methods such as small and ultra-small angle neutron scattering (SANS and USANS, respectively), yield unique, pore-size-specific insights into the kinetics of CO_2 sorption in a wide range of pores (nano to meso). These methods also provide data that may be used to determine the density of adsorbed CO_2

through the evolution of microstructure and adsorption capacity. This approach has been applied to the analysis of CO_2 in geological samples, including coal. By studying coal exposed to CO_2 at subsurface-like temperature and pressure the phase behaviour of the confined CO_2, particularly the densification occurring on changing from the gaseous to the liquid phase, was found to have significant operational and reservoir capacity ramifications when assessing the suitability of unmineable coal seams for use as CO_2 sequestration reservoirs [51]. The results show that the sorption capacity of coal is sample-dependent and strongly affected by the phase state of the injected fluid (subcritical or supercritical). Subcritical CO_2 densifies in the coal matrix, with details of CO_2 sorption differing greatly between different coals and dependent on the amount of mineral matter dispersed in the coal. A purely organic matrix was found to absorb more CO_2 per unit volume than one containing mineral matter, although the mineral matter markedly accelerated the sorption kinetics [52].

Figure 3.6 shows SANS and USANS data for coal from Seelyville (Indiana, USA) exposed to several pressures of CO_2, which could be described using a power law for the scattered intensity with an exponent of −3, indicating the fractal character of the scattering. The scattering intensity shows Q-dependency as a result of the CO_2 in the pores. After completion of the pressure cycling, the neutron-scattering curves returned to their original shapes within 1 %, implying that the microstructure was not permanently affected by exposure to CO_2 over a period of days. This result indicated that the phenomenon of coal plasticization upon exposure to CO_2 may be less widespread than thought previously. The work also found that the small pores within coal are filled preferentially over larger void-spaces by the invading CO_2, a result echoed by MOFs [32]. Apparent diffusion coefficients for CO_2 in coal are thought to vary in the range 5×10^{-7} to more than 10^{-4} cm^2min^{-1} according to the CO_2 pressure and location. At higher pressures CO_2 is shown to

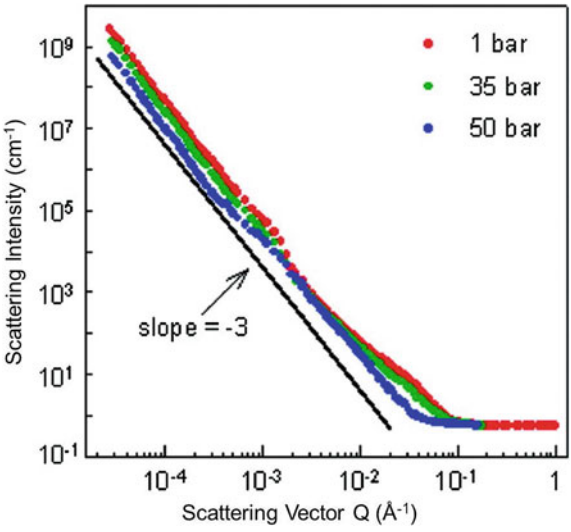

Fig. 3.6 SANS and USANS profiles for Seelyville coal exposed to various pressures of CO_2. Reprinted with permission from (A.P. Radlinski, T.L. Busbridge, E.M. Gray, T.P. Blach, G. Cheng, Y.B. Melnichenko, D.J. Cookson, M. Mastaterz, J. Esterle, Langmuir **25**, 2385 (2009)) [52]. Copyright (2009) American Chemical Society

diffuse immediately into the coal matrix, swelling the coal and changing its macromolecular structure, where it is postulated to create microporosity through the extraction of volatile components [53]. Injection of CO_2 into model subsurface geologic formations has been identified as a key strategy for CO_2 storage. Key to the success of such a strategy is the prevention of leakage from the host by an effective cap with low porosity and permeability characteristics. Shales comprise the majority of caps encountered in subsurface injection sites with pore sizes typically less than 100 nm and whose surface chemistries are dominated by quartz and clays. Analysis of simple, well-characterized fluid-substrate systems can provide details on the thermodynamic, structural, and dynamic properties of CO_2 under conditions relevant to sequestration. In particular, the behaviour of CO_2 interacting with model silica substrates can act as proxies for more complex mineralogical systems. SANS data for CO_2–silica aerogel (95 % porosity; $\sim$7 nm pores) indicates the presence of fluid depletion for conditions above the critical density [54].

3.3 Probing Separations for Post and Pre Combustion Capture, as Well as Oxyfuel Combustion

Currently, postcombustion capture methods, which separate CO_2 at low partial pressures from N_2 in flue streams, are the most economically viable CO_2 capture methods in the short- to mid-term as they can be easily retrofitted to existing power plants. Due to the dilute amount of CO_2 present in these flue-gas streams, prospective materials for this purpose are required to have a high selectivity for CO_2 over N_2, which may be achieved by surface or pore functionalisation with strongly-polarising chemical groups. This may be achieved via the incorporation of open-metal cation sites, often exposed upon desolvation or "activation" of the framework, which provide strong, highly-charged binding sites for CO_2 [55, 56]. Another strategy is the introduction of strongly-polarizing organic functional-groups into the pore. Functional groups investigated previously for CO_2 separation from other gases include amines [22, 57], carboxylic acids, nitro, hydroxy, and sulfone groups [23]. Although more strongly polarizing groups enhance CO_2 adsorption manifested through higher isosteric heats of adsorption, this factor must be balanced against the ease of regenerability of the resulting material in an industrial setting.

3.3.1 Diffusion and Transport of CO_2 and N_2

Silicalite membranes exhibit an interesting selectivity for pure CO_2, which flows through the material faster than He or H_2, notwithstanding the larger kinetic diameter of CO_2 [58]. The diffusion of CO_2 and N_2 in silicalite was studied using QENS, with combined coherent QENS-MD used to determine diffusivities for CO_2

and more traditional QENS used to determine the N_2 diffusivity [59, 60]. The work obtained the diffusivity as a function of intra-crystalline occupancy. A direct comparison between computed and measured transport-diffusion allowed a better understanding of the molecular factors governing the occupancy dependence of the corrected diffusivity, a "pure" kinetic parameter that is largely free of the influence of the isotherm. The corrected diffusivity has often been assumed to be independent of sorbate concentration and approximately equal to the self-diffusivity in the limit of zero occupancy, an assumption that was reassessed in light of these results. These measurements pointed to a significant difference in the occupancy dependence of the corrected diffusivity for N_2 and CO_2, where at 300 K the corrected diffusivity for CO_2 was found to decrease with guest loading of the host and for N_2 at 200 K it was fairly constant, exhibiting a weak maximum. At the practical level this work found that interactions are considerably stronger (more attractive) for CO_2 than for N_2 in silicalite, explaining the strong preference of the material for CO_2.

3.3.2 Probing H_2 Separation from CO_2

Precombustion CO_2 capture in natural-gas plants predominantly involves the separation of CO_2 from H_2 at high pressures, resulting in a pure H_2 stream which is used in energy generation [12]. This process has a component with a higher concentration of CO_2, existing at elevated pressures, resulting in the relatively-low energy penalty for carbon capture of 10–16 % [13]. Additionally, due to the large differences in the polarisability and quadrupole moment between CO_2 and H_2, the two gases are more easily separated via chemical methods than other gases such as CO_2 and N_2 [61]. Porous materials with a high density of localized charge, such as achieved through open-metal sites, are particularly promising for this type of separation. Additionally, variances in gas properties such as diffusion rate may also be exploited by adsorbents to increase selectivity. Aside from selectivity for CO_2, the working capacity of the adsorbent is another major factor in determining the effectiveness of candidate materials for precombustion capture processes. However, these factors are generally inversely related as a material with high selectivity will generally suffer low regenerability as the guest molecules are strongly bound to the adsorbent and are difficult to remove via a mild pressure-swing approach.

Whilst little work exploring H_2 separation specifically from H_2/CO_2 mixtures has been performed using neutron scattering, more work using neutron scattering to study H_2 confined in porous materials has been published than for any other guest molecule. This is a direct consequence of the ease of structural characterization of H (as D) using neutron diffraction as well as the unique information that can be gained for H_2 using neutron spectroscopy [62]. This work is extensive and covered in publications concerning H_2 storage [63, 64], where the interaction of H_2 (D_2) with $Zn_4O(bdc)_3$ (also known as MOF-5) [65, 66], $Cu_3(btc)_2$ [67–71], $Mg_2(dobdc)$ and $Fe_2(dobdc)$ as well as its oxidized analogue [72], $Zn_2(dobdc)$ [73], $Al_2(OH)_2(bptc)$

[74], $Zn(mIm)_2$ where mIm = 2-methylimidazolate and also known as ZIF-8 [75], $Cu_3[Co(CN)_6]_2$ [76], as well as many carbonaceous materials and zeolites, have all been elucidated using neutrons. Such work is the subject of Chap. 8.

3.3.3 Probing N_2 Separation from O_2

Oxyfuel combustion involves the combustion of carbon-based fuels in a pure O_2 stream, however, the limiting factor in the industrial implementation of these methods is the large amount of pure O_2 that is required to be generated from air (O_2/N_2 separation). Microporous solids that are able to efficiently perform this separation have the potential to significantly reduce the large energy-costs currently associated with oxyfuel combustion. Small-pore zeolites have been employed for O_2/N_2 separations by exploitation of the difference in the kinetic diameter between the two gases through physical separation involving molecular sieving. The chemical tunability of the pore space of framework materials, however, facilitates the separation of O_2 and N_2 by taking advantage of the electronic differences between the two gases. In particular, MOFs containing electron-rich redox-active sites, such as $Cr_3(btc)_2$ [77] and $Fe_2(dobdc)$ [78], have been shown to reversibly bind O_2 selectively over N_2 via electron transfer from the metal centre to the O_2.

The $Fe_2(dobdc)$ material binds O_2 preferentially over N_2 at 298 K with an irreversible capacity of 9.3 wt%, corresponding to the adsorption of one O_2 per two Fe centres [78]. Remarkably, at 211 K the O_2 uptake is fully reversible and the capacity increases to 18.2 wt%, corresponding to the adsorption of one O_2 per Fe centre. Mossbauer and infrared spectroscopy measurements indicated partial charge-transfer from the Fe^{II} to the O_2 at low temperature and complete charge-transfer to form Fe^{III} and O_2^{2-} at room temperature. NPD data (4 K) confirm this interpretation, revealing O_2 bound to Fe in a symmetric side-on mode with an O_2 intranuclear separation of 1.25(1) Å at low temperature and of 1.6(1) Å in a slipped side-on mode when oxidized at room temperature (Fig. 3.7).

Similar work reported highly selective and reversible O_2 binding in $Cr_3(btc)_2$ [77], with infrared and X-ray absorption spectra suggesting the formation of an O_2 adduct with partial charge-transfer from the Cr^{II} centres exposed on the surface of the framework. NPD data confirm this mechanism of O_2 binding and indicate a lengthening of the Cr–Cr distance within the "paddle-wheel" units of the framework from 2.06(2) to 2.8(1) Å.

Selectivity for O_2 over N_2 was also achieved in polymer/selective-flake nanocomposite membranes fabricated with a polyimide and a porous layered aluminophosphate. Using SANS to probe the large-scale structure of the O_2/N_2 host material, the substantially improved selectivities of O_2 over N_2 was shown to occur within only 10 wt% of the AlPO layers [79].

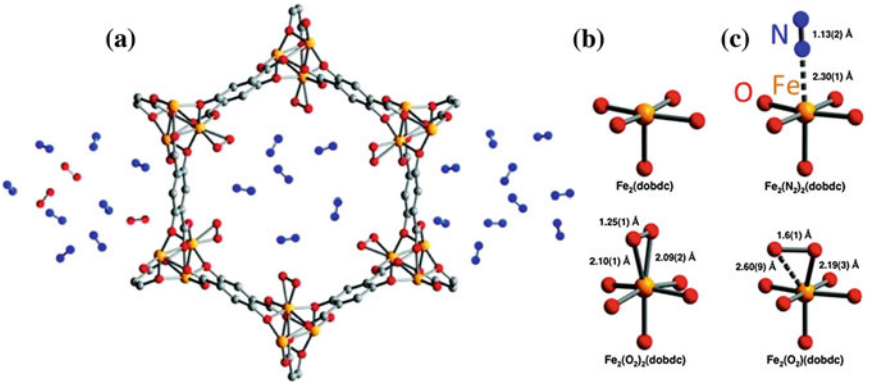

Fig. 3.7 Portion of the crystal structure of Fe_2(dobdc) as viewed approximately along the [001] direction (**a**), where H atoms are omitted for clarity. (**b–e**) First coordination-spheres for the Fe determined from NPD data, where structures are for Fe_2(dobdc) under vacuum (**b**), dosed with N_2 at 100 K (**c**), dosed with O_2 at 100 K (**d**), and dosed with O_2 at 298 K (**e**). Values in parentheses are estimated standard deviations in the final digit. Reprinted from (E.D. Bloch, L.J. Murray, W.L. Queen, S. Chavan, S.N. Maximoff, J.P. Bigi, R. Krishna, V.K. Peterson, F. Grandjean, G.J. Long, B. Smit, S. Bordiga, C.M. Brown, J.R. Long, J. Am. Chem.Soc. **133**, 14814 (2011)) [78]

3.3.4 Probing CO_2/CH_4 Separation for Natural-Gas Sweetening

Natural-gas sweetening (separation of CO_2 from CH_4) is an industrially significant separation process as CO_2 represents a substantial (up to 70 %) impurity in natural-gas wells [80]. The presence of CO_2 reduces the energy content of the natural gas, and its acidity in the presence of water can result in the corrosion of natural-gas lines. Physical solvent-based processes for CO_2 removal from natural-gas are abundant, however, the large amount of water recycling needed makes solvent-based processes highly limited in this application due to solvent degradation and loss during operation [81]. Porous solids present a more efficient and environmentally friendly way to capture CO_2 from natural-gas wells. In this case, separation largely proceeds based on quadrupole moment, due to the similar properties of the two gases in other respects (kinetic diameter, polarizability, dipole moment). Additionally, the flexible structure of some MOFs upon adsorption–desorption (in contrast with "rigid" adsorbents such as carbons and zeolites), may result in dynamic and stepwise adsorption at different pressures. This is generally known as a "gate opening" phenomenon, and arises mainly from the flexibility of the networks and their affinity for particular guests [82]. In MIL-53 [Cr(OH)(bdc)], for example, the selective adsorption of CO_2 over CH_4 is strongly affected by the presence of water which causes dramatic changes in the pore structure [27].

Neutron scattering has also been used extensively to study CH_4 confined in porous materials, in particular to study methane confined in MOFs, commensurate

with the increasing work investigating these hosts for application in CO_2/CH_4 separations.

The metal sites, including open-metal sites, in many MOFs also interact with CH_4. NPD studies of the Mg_2(dobdc) material show the binding of one CD_4 molecule per open-metal site, resulting in the large CH_4 storage capacity of 160–174 cm^3(at standard temperature and pressure, STP)/cm^3, approaching the DOE target of 180 cm^3(STP)/cm^3 for solid-based CH_4 storage at room temperature [83]. Direct determination of CD_4 sorption sites in $Zn(mIm)_2$ and $Zn_4O(bdc)_3$ were gained using NPD (Fig. 3.8) [84]. The primary CD_4 adsorption sites are associated with the organic linkers in $Zn(mIm)_2$ and the metal oxide clusters in $Zn_4O(bdc)_3$. In $Zn_4O(bdc)_3$ the first binding sites ("cup" sites) were not found to alter the $Fm\bar{3}m$ symmetry of the host–guest system. CD_4 at these primary sites possesses well-defined orientations, implying relatively-strong binding with the framework. With higher CD_4 loading, additional CD_4 molecules populate secondary sites and are confined in the framework. The confined CD_4 at these secondary sites is orientationally disordered and stabilized by the intermolecular interactions. The CD_4 guest is a high symmetry guest whose ordered location (at the primary sites) significantly alters the symmetry of system. The "hex" and "ZnO_2" CD_4 sites caused a symmetry lowering of the system to *I4/mmm* as a result of the symmetry incompatibility of the tetrahedral CD_4 molecules with the local geometry. At higher CD_4 loadings a *P*4 *mm* structure was found, where CD_4 sites aligned themselves along the *c* axis and further lowered the symmetry.

Using a similar approach, a comprehensive mechanistic study of CD_4 was performed in $Cu_3(btc)_2$, Cu_2(sbtc) where sbtc = *trans*-stilbene-3, 3′, 5, 5′-tetracarboxylate, and Cu_2(adip) where adip = 5, 5′-(9, 10-anthracenediyl)di-isophthalate and also known as PCN-14, allowing a comparison of structures that consist of the same dicopper-paddlewheel secondary-building units (the well-known dicopper acetate unit), but contain different organic linkers, leading to cage-like pores with various sizes and geometries (Fig. 3.9). This work revealed that CD_4 uptake takes place primarily at two types of strong adsorption site: (1) the open Cu sites which exhibit enhanced coulombic attraction toward CD_4, and (2) the van der Waals potential pocket sites in which the total dispersive interactions are enhanced due to the molecule being in contact with multiple "surfaces". Interestingly, the enhanced van der Waals sites are present exclusively in small cages and at the windows to these cages, whereas large cages with relatively flat pore surfaces bind very little CD_4 [85].

The self-diffusion of CH_4 was measured directly using QENS in the isostructural Cr(OH)(bdc) and V(O)(bdc) materials [86]. The hydroxyl groups in Cr(OH)(bdc) were expected to hinder CH_4 mobility, although this work revealed a global one-dimensional diffusion mechanism of CH_4 in both materials, echoing the single-file diffusion regime found for CO_2 [49]. An interesting result of this work was that CH_4 diffusivities are significantly higher in V(O)(bdc) than in Cr(OH)(bdc) over the whole range of investigated CH_4 loadings.

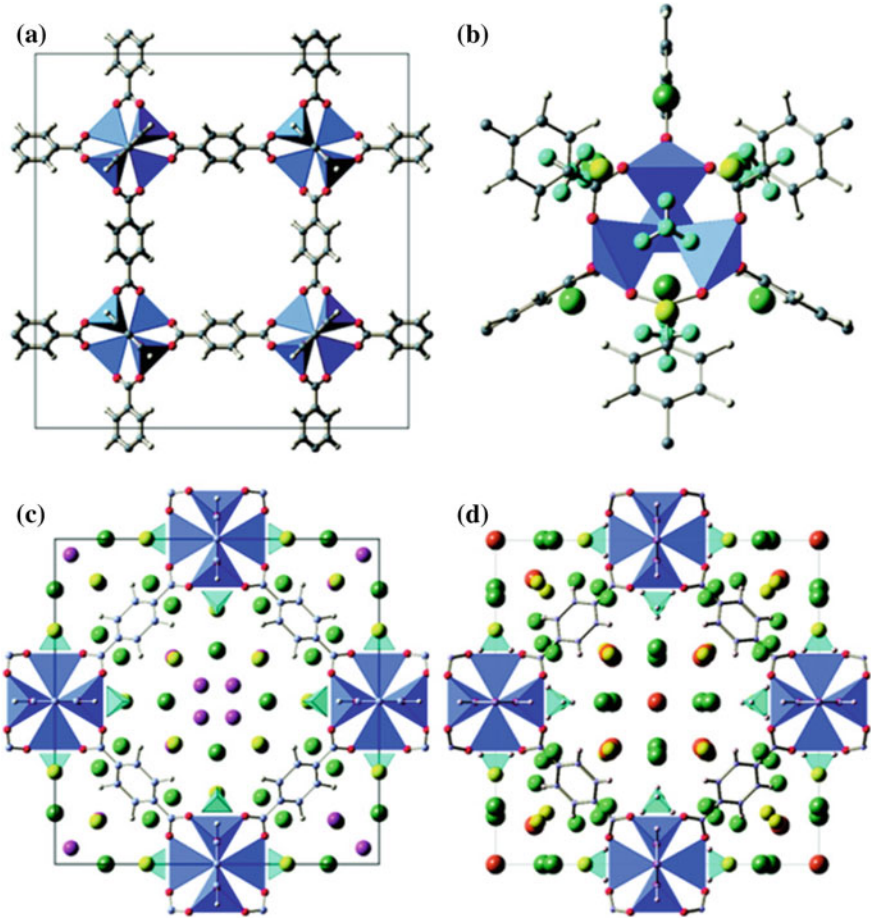

Fig. 3.8 Crystal structure of $Zn_4O(bdc)_3$, with ZnO_4 tetrahedra (*blue*) connected by bdc linkers (**a**). C is grey and D is white. CD_4 adsorption sites in $Zn_4O(bdc)_3$: "cup" sites for the first adsorbed CD_4 with well-defined molecular orientations (cyan) and secondary "hex" (*yellow*) and "ZnO_2" sites (*green*) (**b**). [001] view of *I4/mmm* $Zn_4O(bdc)_3$ with CD_4, additional CD_4 (*pink*) were observed near the pore centre (**c**). [001] view of *P*4 *mm* $Zn_4O(bdc)_3$, where CD_4 sites (*orange*) align along the *c* axis (**d**). Orientationally-disordered CD_4 are shown as spheres for clarity. Reprinted with permission from (H. Wu, W. Zhou, T. Yildirim, J. Phys. Chem. C **113**, 3029 (2009)) [84]. Copyright (2009) American Chemical Society

There have been several neutron-scattering studies targeting the separation mechanism of CO_2 from CH_4. The polymer/selective-flake nanocomposite membranes exhibiting selectivity for O_2 over N_2 (discussed in Sect. 3.3.3) also shows substantial selectivity of CO_2 over CH_4. Again, SANS results revealed that this occurs within only 10 wt% of the AlPO layers. The $Zr_6O_4(OH)(bdc)_6$ material, also known as UiO-66(Zr), is a MOF with encouraging properties for CO_2/CH_4 gas separation, achieved by combining good selectivity with a high working capacity

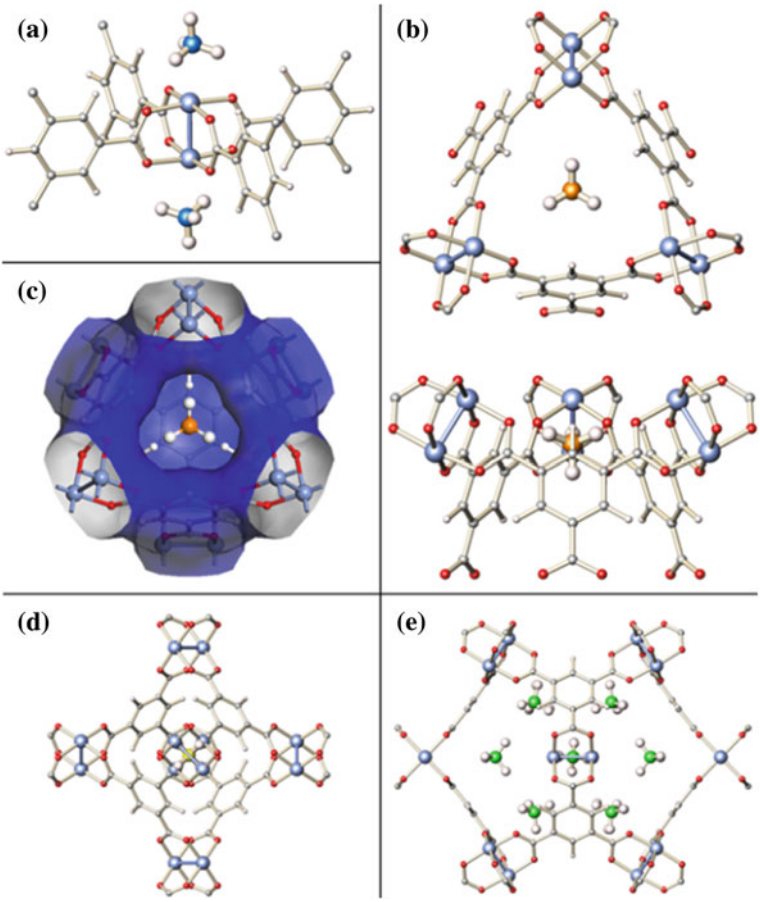

Fig. 3.9 $Cu_3(btc)_2$ with CD_4 molecules adsorbed at the open-Cu sites (**a**) and the small cage window sites (*top and side views*) (**b**). van der Waals surface of the small octahedral-cage, showing the size and geometry of the pore window in excellent match with a methane molecule (**c**). CD_4 molecule adsorbed at the secondary adsorption-site, the centre of the small octahedral-cage (**d**). CD_4 molecule located at the large cage corner-site, also a weak adsorption-site (**e**). C atoms of the CD_4 at different adsorption-sites are colored differently: Open-Cu site is blue, the small cage window-site is orange, the small cage centre site is yellow, and the large cage corner-site is green. Figure adapted from (H. Wu, J.M. Simmons, Y. Liu, C.M. Brown, X.S. Wang, S. Ma, V.K. Peterson, P.D. Southon, C.J. Kepert, H.C. Zhou, T. Yildirim, W. Zhou, Chem. -Eur. J. **16**, 5205 (2010)) [85]

and the ability for regeneration under relatively-mild conditions [87]. $Zr_6O_4(OH)(bdc)_6$ is built from $Zr_6O_4(OH)_4$ octahedra that extend into three-dimensions via bdc ligands, resulting in two types of microporous cages. The dynamics of CO_2 and CH_4 within $Zr_6O_4(OH)(bdc)_6$ was measured using QENS and matched with results from MD simulations [87] (Fig. 3.10). Importantly, this work established the

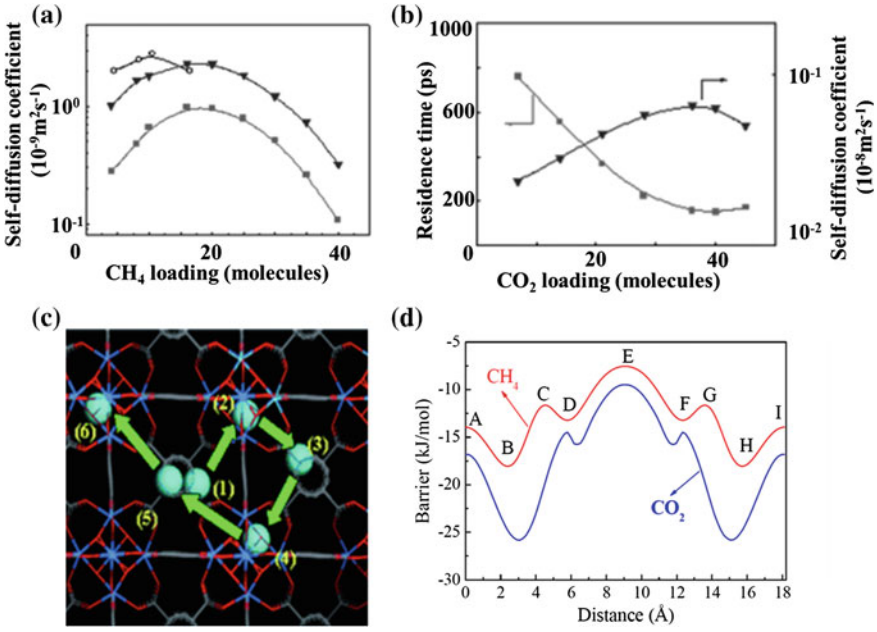

Fig. 3.10 Evolution of self-diffusion coefficients of CH_4 in $Zr_6O_4(OH)(bdc)_6$ at 230 K as a function of concentration (**a**): QENS (*empty circles*), MD simulations using a rigid (*filled squares*) and flexible (*filled triangles*) framework. Simulated self-diffusivity (*triangles*) of CO_2 in $Zr_6O_4(OH)(bdc)_6$ at 230 K as a function of concentration (**b**). The residence times (*squares*) for CO_2 molecules in the tetrahedral cages of $Zr_6O_4(OH)(bdc)_6$ are also shown. Typical illustration of the CH_4 diffusion mechanism in $Zr_6O_4(OH)(bdc)_6$ (**c**). Positions 1–6 correspond to jump sequences of CH_4 in the MD calculations. Potential-energy distribution for a CH_4 (*upper*) and CO_2 (*lower*) in $Zr_6O_4(OH)(bdc)_6$ as it passes from the centre of one tetrahedral cage to another, via the centre of the octahedral cage (d). Reprinted from (Q.Y. Yang, H. Jobic, F. Salles, D. Kolokolov, V. Guillerm, C. Serre, G. Maurin, Chem. -Eur.J. **17**, 8882 (2011)) [87] with permission

concentration dependence of the diffusivities of CH_4 and CO_2 (self and transport, respectively) within the material. The flexibility of the framework was found to influence significantly the diffusivity of the two species, and CH_4 was found to diffuse faster than CO_2 over a broad concentration range, a result that is in contrast to zeolites with narrow windows, for which opposite trends were observed. Further analysis of the MD trajectories for CH_4 provided insights into the global microscopic diffusion-mechanism, proposed to occur by a combination of intracage motions and jump sequences between the material's tetrahedral and octahedral cages. The coadsorption of CO_2 and CH_4 in the material, from both a thermodynamic and a kinetic perspective, was also studied using this approach. It was shown that each type of guest adsorbs preferentially in the two different pores, where CO_2 occupies the tetrahedral cages and CH_4 the octahedral cages. Further, a very unusual dynamic behaviour was also noted in the study of CH_4/CO_2 mixtures in $Zr_6O_4(OH)(bdc)_6$ in that the slower CO_2 molecule was found to enhance the

mobility of the faster CH_4, again contrasting with the usual observation for CO_2/CH_4 mixtures in narrow-window zeolites, where the molecules diffuse independently or slow the partner species.

The self-diffusion properties of pure CH_4 and its binary mixture with CO_2 within the NaY zeolite have also been investigated by the combined QENS/MD approach. This material combines several favourable features including a good selectivity, high working capacity, and potential easy regenerability that make it a good candidate for the selective adsorption of CO_2 over CH_4 [88]. The QENS measurements at 200 K led to an unexpected self-diffusivity profile for pure CH_4 with the presence of a maximum for a loading of 32 CH_4/unit cell, which was previously unobserved for the diffusion of an apolar species in a zeolite with large windows. The QENS measurements report only a slight decrease of the self-diffusivity of CH_4 in the presence of CO_2 when the CO_2 loading increases. MD calculations successfully reproduce this experimental trend and suggest a microscopic diffusion-mechanism in the case of this binary mixture [89].

3.4 Experimental Challenges and the Importance of In Situ Experimentation

The analysis of porous materials and their interaction with guest molecules using neutron scattering is experimentally challenging. Even with advances in neutron sources and instrumentation, several hundred milligrams of material are usually required for successful neutron-scattering analysis of these systems. Evacuated materials prepared for guest sorption are air-sensitive, mandating their handling in specialist atmospheres such as a helium-filled glove box, where helium is necessary to avoid the heat-transfer medium freezing where the heat-transfer gas is not removed from activated samples prior to low-temperature (<10 K) measurement.

Obtaining a good neutron-scattering signal from the host or guest being studied can involve isotopic substitution, and often with complex ligands that require deuteration. The requirement of neutrons in this work is demonstrated by the recent synthesis of deuterated forms of complex ligands, such as 4, 4′, 4″-benzene-1, 3, 5-triyl-tribenzoic acid, through a technique developed at a specialist deuteration facility associated with a neutron-scattering centre. Such complex chemical synthetic routes are achievements in their own right [90].

The majority of neutron-scattering experiments exploring guest-host interactions in porous adsorbents are in situ in nature. The in situ approach, however, varies in accordance to the experimental need. Most commonly activated materials (porous materials with their pores empty) are analysed at low temperature first, before the introduction of guest molecules to the sample at a temperature where the guest will remain in the gaseous state, and the sample is then cooled slowly to where the guest molecules “lock in” to their equilibrium positions, before the measurement continues. These measurements involve careful control of the temperature of the

sample as well as gas-delivery lines through the use of modified cryofurnaces. Advances in neutron instrumentation, particularly large area-detectors and higher-intensity sources, provide the opportunity to resolve in real-time details for such systems [91].

3.5 Perspectives for Neutron Scattering in the Study of Porous Materials for CO_2 Separation, Capture, and Storage

Clearly, the development of more efficient, cost-effective, and industrially-viable CO_2 capture materials is essential for the deployment of large-scale CCS. Novel concepts for porous hosts used for CO_2 capture and separation require a molecular level of control that can take advantage of differences in the chemical reactivity of gas molecules. A challenge in the capture of CO_2 is tuning the selectivity of adsorbents, and coupled with this is the need to examine the adsorption selectivity at the molecular level. Neutron scattering has made important contributions in the understanding of the fundamental separation and storage mechanisms underpinning the functionality of porous materials used in CO_2 capture processes. Great potential exists to develop porous hosts for this purpose using neutron scattering by probing adsorption sites, as well as guest orientation, dynamics, and diffusion in wide range of porous materials. Additionally, the characterization of the hosts themselves and their response to guest adsorption, both on a crystallographic and large-scale structure scale is important.

Postcombustion capture from power-plant flue streams provides one strategy towards reducing CO_2 emissions to the atmosphere, however, there is an urgent need for new methods and materials that perform this separation. In contrast to the low pressure, predominantly CO_2/N_2 separation required for postcombustion capture, materials for precombustion (high pressure, predominantly CO_2/H_2) capture and natural-gas sweetening (predominantly CO_2/CH_4), have distinct requirements. Careful consideration must therefore be afforded to the working conditions of the material at which capture occurs in order to tailor the properties of that material. Commensurate with this requirement is the need for studying materials under relevant working conditions, with an emerging area of particular relevance being the understanding of gas transport in mixed gas and vapour streams. Such co-adsorption experiments, performed for CO_2 and CH_4 mixtures [88, 89], could be extended to study important ternary mixtures such as $CO_2/H_2O/N_2$. This would allow derivation of important competitive gas-sorption mechanisms that are difficult to derive using other methods such as sorption analysis and diffuse-reflectance Fourier-transform infrared spectroscopy. This approach can be expanded further to include mixtures representative of separations that are industrially relevant, and for conversion and catalytic reactions.

References

1. A. Neftel, H. Friedli, E. Moor, H. Lötscher, H. Oeschger, U. Siegenthaler, B. Stauffer, *Trends: A Compendium of Data on Global Change, Carbon Dioxide Information Analysis Center.* (Oak Ridge National Laboratory, US Department of Energy, 1994)
2. C.D. Keeling, T.P. Whorf, M. Wahlen, J. van der Plichtt, Nature **375**, 666 (1995)
3. B. Metz, O. Davidson, H. de Coninck, M. Loos, L. Meyer, IPCC special report on Carbon Dioxide Capture and Storage (2005)
4. http://unfccc.int/2860.php. Accessed 4 Mar 2014
5. http://www.usaid.gov/climate. Accessed 4 Mar 2014
6. K. Sumida, D.L. Rogow, J.A. Mason, T.M. McDonald, E.D. Bloch, Z.R. Herm, T.-H. Bae, J.R. Long, Chem. Rev. **112**, 724 (2011)
7. D.M. D'Alessandro, B. Smit, J.R. Long, Angew. Chem. Int. Ed. **49**, 6058 (2010)
8. J.D. Figueroa, T. Fout, S. Plasynski, H. McIlvried, R.D. Srivastava, Int. J. Greenh. Gas Control **2**, 9 (2008)
9. C.E. Powell, G.G. Qiao, J. Membr. Sci. **279**, 1 (2006)
10. P.D. Vaidya, E.Y. Kenig, Chem. Eng. Technol. **30**, 1467 (2007)
11. E.P.R. Institute, *Program on technology innovation: post-combustion CO_2 capture technology development* (Electric Power Res. Ins, Palo Alto, 2008)
12. P.H.M. Feron, C.A. Hendriks, Oil and gas science and technology—rev. IFP **60**, 451 (2005)
13. L.I. Eide, D.W. Bailey, Oil and gas science and technology—rev. IFP **60**, 475 (2005)
14. M.M. Abu-Khader, Energ. Source. Part A **28**, 1261 (2006)
15. Q. Yang, C. Zhong, J. Phys. Chem. B **110**, 17776 (2006)
16. R.V. Siriwardane, M.-S. Shen, E.P. Fisher, J.A. Poston, Energ. Fuels **15**, 279 (2001)
17. X. Xu, C. Song, B.G. Miller, A.W. Scaroni, Fuel Process. Technol. **86**, 1457 (2005)
18. J.C. Hicks, J.H. Drese, D.J. Fauth, M.L. Gray, G. Qi, C.W. Jones, J. Am. Chem. Soc. **130**, 2902 (2008)
19. B. Moulton, M.J. Zaworotko, Chem. Rev. **101**, 1629 (2001)
20. C. Janiak, Dalton Trans. **14**, 2781 (2003)
21. A. Demessence, D.M. D'Alessandro, M.L. Foo, J.R. Long, J. Am. Chem. Soc. **131**, 8784 (2009)
22. T.M. McDonald, W.R. Lee, J.A. Mason, B.M. Wiers, C.S. Hong, J.R. Long, J. Am. Chem. Soc. **134**, 7056 (2012)
23. E. Neofotistou, C.D. Malliakas, P.N. Trikalitis, Chem.-Eur. J. **15**, 4523 (2009)
24. D.N. Dybtsev, H. Chun, S.H. Yoon, D. Kim, K. Kim, J. Am. Chem. Soc. **126**, 32 (2003)
25. B. Chen, S. Ma, E.J. Hurtado, E.B. Lobkovsky, H.-C. Zhou, Inorg. Chem. **46**, 8490 (2007)
26. B. Chen, S. Ma, F. Zapata, F.R. Fronczek, E.B. Lobkovsky, H.-C. Zhou, Inorg. Chem. **46**, 1233 (2007)
27. P.L. Llewellyn, S. Bourrelly, C. Serre, Y. Filinchuk, G. Férey, Angew. Chem. Int. Ed. **45**, 7751 (2006)
28. C. Serre, S. Bourrelly, A. Vimont, N.A. Ramsahye, G. Maurin, P.L. Llewellyn, M. Daturi, Y. Filinchuk, O. Leynaud, P. Barnes, G. Férey, Adv. Mater. **19**, 2246 (2007)
29. P.D.C. Dietzel, R.E. Johnsen, H. Fjellvag, S. Bordiga, E. Groppo, S. Chavan, R. Blom, Chem. Commun. **41**, 5125 (2008)
30. R. Vaidhyanathan, S.S. Iremonger, G.K.H. Shimizu, P.G. Boyd, S. Alavi, T.K. Woo, Science **330**, 650 (2010)
31. M.R. Hudson, W.L. Queen, J.A. Mason, D.W. Fickel, R.F. Lobo, C.M. Brown, J. Am. Chem. Soc. **134**, 1970 (2012)
32. H. Wu, J.M. Simmons, G. Srinivas, W. Zhou, T. Yildirim, J. Phys. Chem. Lett. **1**, 1946 (2010)
33. W.L. Queen, C.M. Brown, D.K. Britt, P. Zajdel, M.R. Hudson, O.M. Yaghi, J. Phys. Chem. C **115**, 24915 (2011)
34. T.A. Steriotis, K.L. Stefanopoulos, F.K. Katsaros, R. Glaser, A.C. Hannon, J.D.F. Ramsay, Phys. Rev. B **78**, 115424 (2008)

35. K.L. Stefanopoulos, T.A. Steriotis, F.K. Katsaros, N.K. Kanellopoulos, A.C. Hannon, J.D.F. Ramsay, in *5th European Conference on Neutron Scattering*, vol. 340. (Iop Publishing Ltd, Bristol, 2012)
36. T.A. Steriotis, K.L. Stefanopoulos, N.K. Kanellopoulos, A.C. Mitropoulos, A. Hoser, Colloid Surf. A-Physicochem. Eng. Asp. **241**, 239 (2004)
37. H. Wu, J.M. Simmons, G. Srinivas, W. Zhou, T. Yildirim, J. Phys. Chem. Lett. **1**, 1946 (2010)
38. R.K. Motkuri, P.K. Thallapally, B.P. McGraii, S.B. Ghorishi, Cryst. Eng. Comm. **12**, 4003 (2010)
39. S.H. Ogilvie, S.G. Duyker, P.D. Southon, V.K. Peterson, C.J. Kepert, Chem. Commun. **49**, 9404 (2013)
40. T. Ikeda, O. Yamamuro, T. Matsuo, K. Mori, S. Torii, T. Kamiyama, F. Izumi, S. Ikeda, S. Mae, J. Phys. Chem. Solids **60**, 1527 (1999)
41. N. Igawa, T. Taguchi, A. Hoshikawa, H. Fukazawa, H. Yamauchi, W. Utsumi, Y. Ishii, J. Phys. Chem. Solids **71**, 899 (2010)
42. A. Falenty, G. Genov, T.C. Hansen, W.F. Kuhs, A.N. Salamatin, J. Phys. Chem. C **115**, 4022 (2011)
43. A.J. Ramirez-Cuesta, Comput. Phys. Commun. **157**, 226 (2004)
44. S. Yang, J. Sun, A.J. Ramirez-Cuesta, S.K. Callear, W.I.F. David, D.P. Anderson, R. Newby, A.J. Blake, J.E. Parker, C.C. Tang, M. Schröder, Nat. Chem. **4**, 887 (2012)
45. H. Jobic, D.N. Theodorou, Microporous Mesoporous Mat. **102**, 21 (2007)
46. H. Jobic, K. Makzodimitris, G.K. Papadopoulos, H. Schober, D.N. Theodorou, in *Proceedings of the 14th International Zeolite Conference*, Cape Town, 2004
47. D. Plant, H. Jobic, P. Llewellyn, G. Maurin, Eur. Phys. J. -Spec. Top. **141**, 127 (2007)
48. F. Salles, H. Jobic, T. Devic, P.L. Llewellyn, C. Serre, G. Ferey, G. Maurin. ACS Nano **4**, 143 (2010)
49. F. Salles, H. Jobic, A. Ghoufi, P.L. Llewellyn, C. Serre, S. Bourrelly, G. Ferey, G. Maurin. Angew. Chem. Int. Ed. **48**, 8335 (2009)
50. A.V. Neimark, F.-X.Coudert, C. Triguero, A. Boutin, A.H. Fuchs, I. Beurroies, R. Denoyel, Langmuir, **27**, 4734 (2011)
51. Y.B. Melnichenko, A.P. Radlinski, M. Mastalerz, G. Cheng, J. Rupp, Int. J. Coal Geol. **77**, 69 (2009)
52. A.P. Radlinski, T.L. Busbridge, E.M. Gray, T.P. Blach, G. Cheng, Y.B. Melnichenko, D.J. Cookson, M. Mastaterz, J. Esterle, Langmuir, **25**, 2385 (2009)
53. M. Mirzaeian, P.J. Hall, H.F. Jirandehi, J. Mater. Sci. **45**, 5271 (2010)
54. D.R. Cole, A.A. Chialvo, G. Rother, L. Vlcek, P.T. Cummings, Philos. Mag. **90**, 2339 (2010)
55. P.D.C. Dietzel, R.E. Johnsen, R. Blom H. Fjellvåg, Chem.-Eur. J. **14,** 2389 (2008)
56. E.D. Bloch, D. Britt, C. Lee, C.J. Doonan, F.J. Uribe-Romo, H. Furukawa, J.R. Long, O.M. Yaghi, J. Am. Chem. Soc. **132**, 14382 (2010)
57. J. An, S.J. Geib, N.L. Rosi, J. Am. Chem. Soc. **132**, 38 (2009)
58. M.E. Welk, F. Bonhomme, T.M. Nenoff, Prepr. Pap. -Am. Chem. Soc. Div. Fuel Chem., **49,** 245 (2004)
59. H. Jobic, K. Makrodimitris, G.K. Papadopoulos, H. Schober, D.N. Theodorou, in *Recent Advances in the Science and Technology of Zeolites and Related Materials*, Pts a—C, eds. by E. VanSteen, M. Claeys and L. H. Callanan, vol. 154. (Elsevier Science Bv, Amsterdam, 2004) pp. 2056
60. G.K. Papadopoulos, H. Jobic, D.N. Theodorou, J. Phys. Chem. B **108**, 12748 (2004)
61. J.-R. Li, R.J. Kuppler, H.-C. Zhou, Chem. Soc.Rev. **38**, 1477 (2009)
62. A.J. Ramirez-Cuesta, M.O. Jones, W.I.F. David, Mater. Today **12**, 54 (2009)
63. M. Hirscher (ed.), *Handbook of Hydrogen Storage, New Materials for Future Energy Storage* (WILEY-VCH, Weinheim, 2010)
64. P. Earis, ed., *Hydrogen Storage Materials*, (RSC Publishing, 2011)
65. T. Yildirim, M.R. Hartman, Phys. Rev. Lett., 95 (2005)
66. F.M. Mulder, T.J. Dingemans, H.G. Schimmel, A.J. Ramirez-Cuesta, G.J. Kearley, Chem. Phys. **351**, 72 (2008)

67. V.K. Peterson, C.M. Brown, Y. Liu, C.J. Kepert, J. Phys. Chem. C **115**, 8851 (2011)
68. V.K. Peterson, Y. Liu, C.M. Brown, C.J. Kepert, J. Am. Chem. Soc. **128**, 15578 (2006)
69. V.K. Peterson, Y. Liu, C.M. Brown, C.J. Kepert, Mater. Res. Soc. **561–565**, 1601 (2007)
70. C.M. Brown, Y. Liu, T. Yildirim, V.K. Peterson, C.J. Kepert, Nanotechnology, 20 (2009)
71. Y. Liu, C.M. Brown, D.A. Neumann, V.K. Peterson, C.J. Kepert, J. Alloy, Compd **446**, 385 (2007)
72. W.L. Queen, E.D. Bloch, C.M. Brown, M.R. Hudson, J.A. Mason, L.J. Murray, A.J. Ramirez-Cuesta, V.K. Peterson, J.R. Long, Dalton T. **41**, 4180 (2012)
73. Y. Liu, H. Kabbour, C.M. Brown, D.A. Neumann, C.C. Ahn, Langmuir **24**, 4772 (2008)
74. X. Lin, I. Telepeni, A.J. Blake, A. Dailly, C.M. Brown, J.M. Simmons, M. Zoppi, G.S. Walker, K.M. Thomas, T.J. Mays, P. Hubberstey, N.R. Champness, M. Schroder, J. Am. Chem. Soc. **131**, 2159 (2009)
75. H. Wu, W. Zhou, T. Yildirim, J. Am. Chem. Soc. **129**, 5314 (2007)
76. M.R. Hartman, V.K. Peterson, Y. Liu, S.S. Kaye, J.R. Long, Chem. Mater. **18**, 3221 (2006)
77. L.J. Murray, M. Dinca, J. Yano, S. Chavan, S. Bordiga, C.M. Brown, J.R. Long, J. Am. Chem. Soc. **132**, 7856 (2010)
78. E.D. Bloch, L.J. Murray, W.L. Queen, S. Chavan, S.N. Maximoff, J.P. Bigi, R. Krishna, V.K. Peterson, F. Grandjean, G.J. Long, B. Smit, S. Bordiga, C.M. Brown, J.R. Long, J. Am. Chem. Soc. **133**, 14814 (2011)
79. H.K. Jeong, W. Krych, H. Ramanan, S. Nair, E. Marand, M. Tsapatsis, Chem. Mater. **16**, 3838 (2004)
80. H. Lin, E. Van Wagner, R. Raharjo, B.D. Freeman, I. Roman, Adv. Mater. **18**, 39 (2006)
81. P.D.C. Dietzel, V. Besikiotis, R. Blom, J. Mater. Chem. **19**, 7362 (2009)
82. M. Tagliabue, D. Farrusseng, S. Valencia, S. Aguado, U. Ravon, C. Rizzo, A. Corma, C. Mirodatos, Chem. Eng. J. **155**, 553 (2009)
83. H. Wu, W. Zhou, T. Yildirim, J. Am. Chem. Soc. **131**, 4995 (2009)
84. H. Wu, W. Zhou, T. Yildirim, J. Phys. Chem. C **113**, 3029 (2009)
85. H. Wu, J.M. Simmons, Y. Liu, C.M. Brown, X.S. Wang, S. Ma, V.K. Peterson, P.D. Southon, C.J. Kepert, H.C. Zhou, T. Yildirim, W. Zhou, Chem. -Eur. J. **16**, 5205 (2010)
86. N. Rosenbach, H. Jobic, A. Ghoufi, F. Salles, G. Maurin, S. Bourrelly, P.L. Llewellyn, T. Devic, C. Serre, G. Ferey, Angew. Chem. Int. Ed. **47**, 6611 (2008)
87. Q.Y. Yang, H. Jobic, F. Salles, D. Kolokolov, V. Guillerm, C. Serre, G. Maurin, Chem. -Eur. J. **17**, 8882 (2011)
88. Q.Y. Yang, A.D. Wiersum, H. Jobic, V. Guillerm, C. Serre, P.L. Llewellyn, G. Maurin, J. Phys. Chem. C **115**, 13768 (2011)
89. I. Deroche, G. Maurin, B.J. Borah, S. Yashonath, H. Jobic, J. Phys. Chem. C **114**, 5027 (2010)
90. T.A. Darwish, A.R.G. Smith, I.R. Gentle, P.L. Burn, E. Luks, G. Moraes, M. Gillon, P.J. Holden, M. James, Tetrahedron Lett. **53**, 931 (2012)
91. F.M. Mulder, B. Assfour, J. Huot, T.J. Dingemans, M. Wagemaker, A.J. Ramirez-Cuesta, J. Phys. Chem. C **114**, 10648 (2010)